Accepted Manuscript

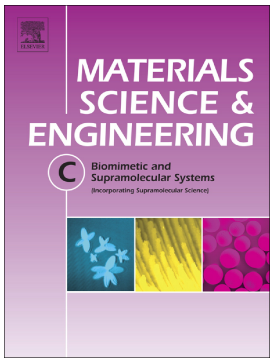


# Microstructured hybrid scaffolds for aligning neonatal rat ventricular myocytes

Ilaria Sanzari, Franco Dinelli, Eleanor Humphrey, Cesare Terracciano, Themistoklis Prodromakis

PII: S0928-4931(18)33448-9
DOI: https://doi.org/10.1016/j.msec.2019.109783
Article Number: 109783
Reference: MSC 109783

To appear in: *Materials Science & Engineering C*

Received date: 12 November 2018
Revised date: 23 April 2019
Accepted date: 20 May 2019

Please cite this article as: I. Sanzari, F. Dinelli, E. Humphrey, et al., Microstructured hybrid scaffolds for aligning neonatal rat ventricular myocytes, Materials Science & Engineering C, https://doi.org/10.1016/j.msec.2019.109783

# Microstructured Hybrid Scaffolds for Aligning Neonatal Rat Ventricular Myocytes

Ilaria Sanzari[a], Franco Dinelli[b], Eleanor Humphrey[c], Cesare Terracciano[c], Themistoklis Prodromakis[d]

[a]School of Engineering, Faculty of Engineering and Physical Sciences, University of Southampton, Southampton SO17 1BJ, United Kingdom

[b]Consiglio Nazionale delle Ricerche (CNR), INO UOS 'A. Gozzini', Area della Ricerca di Pisa - S. Cataldo, via Moruzzi 1, I-56124 Pisa, Italy

[c]National Heart and Lung Institute, Imperial College London, London, United Kingdom

[d]Electronic Materials and Devices Research Group, Zepler Institute for Photonics and Nanoelectronics, University of Southampton, Southampton SO17 1BJ, United Kingdom

**Corresponding author**

ilaria.sanzari@soton.ac.uk

**Abstract**

In cardiac tissue engineering (TE), *in vitro* models are essential for the study of healthy and pathological heart tissues in order to understand the underpinning mechanisms. In this scenario, scaffolds are platforms that can realistically mimic the natural architecture of the heart, and they add biorealism to *in vitro* models. This paper reports a novel and robust technique to fabricate cardiovascular-mimetic scaffolds based on Parylene C and Polydimethylsiloxane (PDMS). Parylene C is employed as a mask material for inducing hybrid and non-hybrid micropatterns to the PDMS layer. Hybrid architectures present striped hydrophobic/hydrophilic surfaces, whereas non-hybrid scaffolds only corrugated topographies. Herein, we demonstrate that wavy features on PDMS can be obtained at the micro- and nanoscale and that PDMS can be integrated into the microfabrication process without changing its intrinsic physical properties. A study of the effects of these scaffolds on the growth of Neonatal Rat Ventricular Myocytes (NRVMs) cultures reveals that cell alignment occurs only for the case of hybrid architectures made of hydrophilic PDMS and hydrophobic Parylene C.

**Keywords:** PDMS, Parylene C, microgrooves, elasticity, NRVM.

## 1 Introduction

It is well known that heart function is strongly correlated to the structural organisation of the heart tissue[1]. Anisotropy is the property of the extracellular environment of cardiomyocytes that influences cell function and the propagation of the action potential [2]. In cardiac TE anisotropic biomaterials are gaining interest to develop scaffolds for *in vitro* models to better understand the fundamental mechanisms induced by such structures on cardiomyocyte maturation [3]. Despite the progress in material science and in tissue engineering, it is still necessary to develop further insights to design more realistic platforms to mimic the physiological environment.

In the past decades, scaffolds with biochemical cues have been widely investigated, but the importance of biophysical effects on cardiomyocytes has come recently into focus as a critical aspect to mimic cardiac microenvironment [4],[5]. Several implementation strategies, such as lithography [6], micro-contact printing [7], electrospinning [8], acoustic electromachining [9] and UV-assisted capillary lithography [10] have been proposed so far for creating anisotropic substrates with feature depths and widths ranging from microscale to the nanoscale[11]. Among them, microfabrication processes are more versatile allowing patterns down to the nanoscale for a wide variety of polymers. For example, elastomers like PDMS can be patterned with high reproducibility, providing substrates with suitable elastic properties [1]. Nonetheless, the patterning of soft materials with excellent control and reliable manner is still elusive, and further investigations are required.

Standard microfabrication is one of the technique generally employed to obtain different topographies [11]. Huang et al. have studied the assembly of myotubes on PDMS and (poly(L-lactide-co-glycolide-co-εcaprolactone) membranes fabricated using soft lithography with 10µm wide, 10µm apart and 2.8µm deep lines [12]. They compared nano- and micro-topographies showing higher myotubes alignment (length 40% longer than on nonpatterned) with well-striated sarcomeres (percentage of striation of almost 60%) only on microgrooves. Altomore et al. followed a similar approach by creating microgrooves on a biodegradable poly-L-lactide/trimethylene carbonate copolymer with different groove widths (5-100µm) and depths (0.5-5µm). They found that grooves with 1µm depth and 25µm width promote proper development of the myotubes [13]. On the other hand, Lam et al. investigated the effects of wrinkles obtained on the surface of PDMS. Surfaces with various wavelengths (3-12µm) and amplitudes (400-1700nm) were fabricated, and applied with C2C12 cells, discovering that the cell plating density needs to be controlled to see a cell alignment effectively. Also, cells on 6µm wavelength features showed a cytoskeleton alignment along the main direction of the waves [14].

In the past few years, Parylene C has been also engineered for cardiac tissue engineering applications using standard microfabrication techniques. Trantidou et al. demonstrated that NRVMs not only are elongated on selective hydrophobic/hydrophilic Parylene C microgrooved surface with an angle of almost 25° but they showed a significant improvement on calcium activity under stimulation of 0.5-2Hz [6]. However, we previously demonstrated that Parylene C is too stiff for mimicking the elastic environment of the heart (Young's modulus equal to 4.85GPa for 8µm [15]) and cells cannot independently beat on such kind of biomaterial.

Therefore, the substrate stiffness is considered as an essential parameter that influences the maturation of NRVMs[16]. Previous studies have presented a maximum contractile force and amplitude of calcium transient using polymers with a stiffness close to the native extracellular matrix (ECM) of the heart[17]. Softer substrates can extensively follow cell contraction regulating the calcium transient shape and the duration of contraction[18]. Among them, PDMS is the most widely exploited polymer. However, this material sometimes behaves unpredictably. For instance, it can crack[19] or form uncontrollable ripples on

the surface[20] especially when it is used for microfabrication process. Even though there is a wide literature on PDMS, its use as a scaffold in TE requires further analysis in applications for *in vitro* platforms.

In this study, we fabricated anisotropic surface structures based on PDMS using Parylene C as masking material. Firstly we collected data demonstrating that the physicochemical properties of PDMS did not change at the nanoscale when prepared as a thin film. We then evaluated the effects of these anisotropic scaffolds on the alignment of NRVMs. Our results show that non-hybrid scaffolds made from corrugated PDMS did not induce cell alignment, whereas hybrid features with hydrophobic Parylene C strips and hydrophilic PDMS trenches enhanced cell alignment.

## 2 Experimental

### *2.1 PDMS substrates preparation*

PDMS Sylgard 184 silicone elastomer kit was purchased from Dow Corning (Barry, UK) and produced in a 10:1 base-to-curing agent ratio as per the manufacturer's instructions. The viscosity of the pre-mixed solution varies with the time and to be consistent with the preparation of the material was monitored over time. The pre-mixed solution was degassed for 40min and then used to prepare the substrates. Bulk substrates were prepared to pour the pre-mixed solution into a 35mm glass petri dish, and after curing, 1cm x 1cm x 1mm small pieces were cut using a laboratory scalpel. PDMS thin films were prepared via a spin coating on 13mm glass coverslips and 6inch glass borosilicate wafers. Three steps of the spin coating were set to have a conformal layer. PDMS pre-solution was spun at 500rpm for the 30s to allow the liquid to cover the substrate uniformly and subsequently the speed was set to half of the target speed for other 30s. The final step defined as the target speed (500-6000rpm) is set for 60s to reach the desired thickness of the PDMS [21]. Four different films were prepared at four different target velocities: 500 (PDMS0.5), 1000 (PDMS1), 4000 (PDMS4) and 6000rpm (PDMS6). All the substrates were cured at 75ºC for 1h and let cooling down overnight before use. We have obtained very thin PDMS membranes down to 8µm as reported in Table 1.

### *2.2 Oxygen plasma treatment*

PDMS1 substrates were exposed to oxygen plasma for 15s in a reactive ion etching (RIE) system (RIE80, Oxford Instruments) with RF power at 13.56MHz. Plasma treatment was done at a power of 200W, pressure 50mTorr and oxygen flow of 10sccm [22]. The exposure to the oxygen plasma of the same category of samples was also performed in an inductively coupled plasma ICP (OPT 100 ICP 380, Oxford Instruments Plasma Technology). These samples were exposed to oxygen plasma for 15s at 1.33Pa pressure, 100sccm flow, 1000W ICP source power and 20W RF power.

### *2.3 Scaffolds fabrication*

In this work we have prototyped three types of microgrooved scaffolds, mimicking the architecture of the heart with grooves 1µm deep and 10µm wide. We have employed Parylene C as masking material to pattern PDMS that is difficult to pattern at the micro-scale. The HH scaffolds present hydrophobic/hydrophilic features on the surface and were fabricated as described in our previous work [15]. The PP1 scaffolds were also fabricated with a corrugated topography made from PDMS [15]. Briefly, Parylene C was firstly patterned with high aspect ratio grooves, then PDMS was spin-coated atop at a high spin speed to obtain wrinkled features 1µm high.

Herein we expand our previous work by presenting the new fabrication of hybrid Parylene C/PDMS scaffolds (PP2) with Parylene C atop PDMS films. Parylene C for these scaffolds has been used to create selectively

hydrophilic elastic areas (PDMS) with stiff hydrophobic ridges (Parylene C). Moreover, in this work Parylene C was used as a mask for exposing PDMS to oxygen plasma.

PDMS1 samples were spin-coated on 6inch borosilicate glass wafers and cured in an oven at 75°C for 1 h (Figure 1.a,b). This thickness was chosen because thick PDMS was shown to improve NRVM elongation and contraction [23]. 900 nm of Parylene C film was then deposited (Figure 1.c), using a commercially available standard Parylene coater (Labcoater PSD2010, SCS). Optical lithography was successively done by spin coating a 1.3µm thick positive photoresist layer (S1813, Microchemicals), soft baking at 110°C for 60s and exposure to UV light (EVG 620 Mask Aligner) for an optimized exposure time of 2s, using a multi-grating dark-field chrome mask, with stripes of 10µm width (Figure 1.d). The crosslinked resist was then developed in MF319 (Microchemicals) and water for 40s (Figure 1.e). Parylene C was then etched in an oxygen plasma using ICP for 1min and 45s (given etching rate approximately 600nm/min) at 1.33Pa pressure, 100sccm flow, 1000W source power and 20W bias power generator. Parylene C, not masked by the resist, was wholly etched until reaching the bottom PDMS areas that were exposed finally to oxygen plasma for almost 15s.

When the etching process was finished, the remaining resist was dissolved in acetone for 5min. In this way, we have obtained PP2 scaffolds with a hybrid surface made by hydrophobic ridges and hydrophilic grooves (Figure 1.g). Finally, the surface of the PP2 constructs was imaged immediately after the fabrication using a LEO 1455VP scanning electron microscope (SEM) and a representative image is shown in Figure 1.h.

After the fabrication HH, PP1 and PP2 were cultured *in vitro* with NRVMs as shown in Figure 1.i,j,k.

### *2.4 Topography characterization*

The topographies of HH, PP1 and PP2 constructs were acquired using Atomic Force Microscopy (AFM), by a Multimode Nanoscope V Veeco in tapping mode. Commercial Al-coated Tap300 Al-G Si tips (Budget Sensors) with resonance frequency ~300Hz and cantilever stiffness ~40N/m were used. 50µm × 50µm areas were captured with a scan rate of 0.8Hz and 512 scanning lines.

The non-hybrid PP1 samples were cut and peeled-off from the wafer. Then they were attached to the AFM sample holder using carbon tape. The HH and PP2 scaffolds were analyzed on squared glass placed on the AFM sample holder. The topography has been quantitatively evaluated as follows: acquisition of three images in three different areas of each sample; same procedure on three samples per each category. Three samples per each fabrication process were analyzed to demonstrate the repeatability of the process. The AFM analysis has been carried out at the centre of each sample.

### *2.5 Chemical characterization*

PDMS surface chemistry before and after oxygen plasma was evaluated by means of Raman spectroscopy. Measurements were taken using a Renishaw's inVia Raman spectrometer (JKR instruments) by exciting 532nm diode laser with 21.8mW beam power and 10s exposure time. A 50X, NA075 (Leica N PLAN EPI 50x/0.75) objective lens was used; giving a laser spot of ~865nm. Data acquisition covers the spectral range 0-3500$cm^{-1}$.

### *2.6 Substrate contact angle*

The surface wettability of PDMS was measured before and after oxygen plasma (almost 1h after the treatment). A 5µl drop of deionised water (R~18MΩ cm) was engaged gradually on the centre of each PDMS substrate and photographed using a highspeed camera. The shape of the drop was then analysed using a Drop

Shape Analysis System (DSA 30 Kruss Co., Germany). The software uses a fitting of a polynomial function that adapts across the baseline of the drop connecting the left and right three-phase points. The angle of the baseline at the right ($\theta_R$) and left ($\theta_L$) side of the droplet at the three-phase point provides the estimated value of the contact angle. Measurements were performed on three different samples, and the values were averaged. The contact angle of each sample was evaluated at the same position before treatment, immediately after treatment and once every day to investigate the longevity of the oxygen plasma treatment over time. Samples were stored in constant and controlled laboratory conditions. Before and after each measurement samples were blown off with nitrogen gun to remove residual water and possible dust particles.

### *2.7 PDMS elasticity test*

The mechanical properties of PDMS were tested at the micro-scale using AFM. Sixteen AFM measurements in an area of 8µm x 8µm were taken before relocating the cantilever to a different region for sixteen more measurements, which has been repeated three or more times per substrate. PDMS bulk, PDMS1, PDMS4 and PDMS6 films were tested in water using a hybrid system made of a commercial head (SMENA, NT-MDT) with home-built electronics. A spherical tip with 5µm of diameter (SQUBE, CP-CONT-BSG-A) has been employed to lead large contact area as illustrated in n Figure 2.a Cantilever spring constant (k) calibration has been performed according to the work of Sader et al. [24] and estimated to be 0.2N/m with an error of 10%.

Firstly, a reference force-distance curve is recorded on a stiff substrate (petri dish bottom). Samples are then placed in a petri dish of 35mm of diameter filled with water. Force-displacement curves were obtained at a rate of 2000nm/s. The Young's modulus has been obtained using the Derjaguin Muller Toporov (DMT) theory that takes into account the adhesion forces and Hertzian contact [25]. The DMT equation applied is the following [26]:

$$F = F_n + F_a = \frac{4ER^{\frac{1}{2}}\delta^{\frac{3}{2}}}{3(1-\nu^2)} \quad (1)$$

Where F is the indentation force, $F_n$ is the normal force, $F_a$ is the adhesive force, R is the radius of the spherical tip, ν is the Poisson's ratio assumed to be 0.5 [27] and δ is the indentation depth calculated as [28]:

$$\delta = \Delta D - \Delta Z \quad (2)$$

ΔD is the absolute deflection relative to the force-free cantilever deflection, and Z is the piezo position as indicated in Figure 2.b. The cantilever deflection and the sample deformation can be only calculated based on the piezo distance that is measured during the nanoindentation tests. To derive the tip-sample separation, the cantilever deflection is calculated as the indentation force divided by the cantilever stiffness.

### *2.8 Substrates preparation for cell culturing*

Before seeding scaffolds were sterilizing in 70% ethanol for 10min and flashed multiple times with phosphate-buffered (PBS) saline solution and water. Type IV human placenta collagen (Sigma-Aldrich) was diluted in 22mL of HBSS and 3mL of glacial acetic acid. The substrates were coated with this solution for 1min, dried and washed with sterile DI water. The samples were finally stored in water and left in a 37°C, 5%$CO_2$ incubators for 1h. PP1 substrates were also sterilized under UV light for 4h before use.

### *2.9 NRVM culture*

Primary cardiomyocyte cultures of NRVMs were obtained from neonatal rats according to schedule 1 regulations (Scientific Procedures) Act 1986. In this study ethics review was not required. Hearts were removed, and cells were isolated from two days old neonatal Sprague-Dawley rats. Cells were then enzymatically digested and filtered to remove undigested tissue, and then fibroblasts removed. NRVMs were collected and counted using a hemocytometer. Almost $100*10^3$ cells in the 20µL medium were then plated on the collagen-coated substrates and experiments were performed at 3-4 days post seeding.

### *2.10 Cell alignment evaluation*

Cell alignment was quantified using immunofluorescence imaging. The sarcomeric structure of the cells was labelled by the monoclonal anti-*α*-actinin antibody (Sigma, A7811) and deoxyribonucleic acid 4', 6-diamidino-2-phenylindole (DAPI) (Invitrogen) was used to label nuclei fluorescently. Fluorescent images were taken using an inverted Zeiss LSM-780 confocal microscope with an x40 oil-immersion lens (Carl Zeiss). The nuclear alignment was determined using Image J software as described elsewhere [29],[30].

Cell morphology and nuclear alignment were evaluated using Image J software (National Institutes of Health, Bethesda, MD). The nuclear alignment was estimated as the lack of deviation in the axis of an individual nucleus from the mean axis of all individual nuclei as reported by Rao et al. [31]. Cell area and aspect ratio (long axis/short axis) were calculated for all cardiomyocytes by manually outlining cells in ImageJ.

### *2.11 Statistical analysis*

Three measurements were taken per each experiment and expressed as a mean ± standard error. For the cell alignment three independent tests were performed (n=3) and results were compared using a Student's t-test assuming the significance when $p<0.05$; the analysis was performed using Prism 4 software (GraphPad Software Inc.). Cellular aspect ratio and area were evaluated from three images of different areas, for three different samples, in order to analyse at least 90 cells. The statistical analysis was performed by using an unpaired t-test (two-tailed), assumed to be significant when $p \leq 0.01$.

## 3 Results and discussion: physicochemical properties of scaffolds and application with cells

### *3.1 Comparison of the topographical features*

In *in vitro* cardiac tissue models, cell alignment is necessary to improve cell maturation and function. Mimicking the anisotropy of the heart tissue is fundamental for the propagation of the action potentials to pin a specific direction and thus greatly improves the electrical conduction of cardiomyocytes [32]. The common technique used to induce cellular alignment consists of surface patterning [33],[34].

Previous studies have demonstrated that NRVMs can significantly align (modulus of the angle of the cell from the mean axis approximately 25°) along the direction of the lines created on HH scaffolds with the depth of almost 1µm [6]. However, these scaffolds were not matching the mechanical conditions of the myocardium and cells were mainly aligned by growing on the hydrophilic channels that were very stiff with Young's modulus of the Parylene C of almost 3 GPa [15].

In this work, Parylene C was considered a good material to pattern PDMS which has 'soft' mechanical properties, alleviating the challenges of handling PDMS solely as a thin film. Following from previous works we argue that PDMS wave topographies may enable not only the alignment of cardiac cells but also the efficient formation of more mature cells with well-aligned sarcomeres [2],[14]

We fabricated relatively shallow topographies, as we believe they may resemble the natural state of the tissue allowing more connections between cells. The width of the grooves has been selected to 10µm based on prior experiments [6], and the height of the grooves was fixed to 1µm since previous findings demonstrated that NRVMs align significantly along the direction of the lines with a depth ranging from 0.5 to 2µm [6],[12]. Also, we believe that these features tempt to mimic the topographical structures imparted by the ECM to cardiomyocytes *in vivo*.

To quantitatively evaluate the accuracy of the fabrication process the profiles of the AFM images were extracted and compared for three microfabrication processes. The AFM images illustrated in Figure 3.a,b,c, show the topographies of HH, PP1 and PP2 scaffolds. The height profiles relative to each topography are reported in Figure 3.d,e,f, showing the period and height of the feature of each scaffold. We observed regular profiles for all the processes relative to each scaffold confirming the repeatability. Table 2 reports the data derived for the three scaffolds. Pitches were evaluated for HH and PP2 constructs while the wavelength was determined for PP1 scaffolds. The wavelength is measured as the average distance between two adjacent wave peaks.

We have here demonstrated that it is possible to fabricate hybrid scaffolds with controllable features with a simple process. This process is wafer-based (~110 scaffolds per 6inch wafer), conventional and not time-consuming. In particular, in the case of PP1, we can also control the height of the waves from nano- to microscale as previously demonstrated [15]. In the Supplementary information (Figure S1), we also reported a nanometric AFM topography of PDMS ripples created on Parylene C grooves with a depth of 2µm.

### *3.2 Surface chemistry investigation*

To obtain ridged PDMS surfaces, we needed to spin coat PDMS at high speeds (6000 rpm). Thus we have hypothesised that spin coating might affect the PDMS mechanical properties. This supported by the fact that shear stress can stretch PDMS polymer chains during spin coating and this phenomenon can affect the elastic modulus of PDMS elastic [35]. Raman spectroscopy can be used to study the presence of local stress on amorphous materials because strain induces a shift in the vibration frequencies of the molecules [36].

We have acquired Raman spectra for PDMS films at different speed values (500-6000rpm), but we have not measured any shift in the peaks. The peaks are in the same position with different intensities, due to the different thickness of the material. Figure 4.a shows PDMS spectra for PDMS bulk, PDMS0.5, PDMS1, PDMS4 and PDMS6. Typical PDMS Raman peaks were found to be consistent with the literature [37],[38]. The band between 150 and 300$cm^{-1}$ is always present and corresponds to C-C bending vibrations [39]. The peak at 486$cm^{-1}$, typical for the native PDMS, corresponds to Si-O-Si bonds stretching. Other typical peaks of PDMS were found at 615, 690 and 708$cm^{-1}$ that corresponds to vibration of methyl groups ($–CH_3$ ), $Si–CH_3$ symmetric rocking and Si-C symmetric stretching. Other peaks at 860, 1260 and 1460$cm^{-1}$ are related to -$CH_3$ symmetric rocking, -$CH_3$ symmetric bending and -$CH_3$ asymmetric bending. The two strong peaks at 2907 and at 2966$cm^{-1}$ correspond to symmetric and antisymmetric $–CH_3$ stretching.

Oxygen plasma has extensively been used to improve the hydrophilicity of PDMS surface especially for cell culturing applications [40],[41]. The treatment of oxygen plasma on PDMS change the surface properties by destroying Si-$CH_3$ groups and introducing silanol groups (Si-OH) and alcohol groups (C-OH) [42]. After oxygen plasma, there is also a formation of a silica-like layer ($SiO_x$) (Figure 4.b) whose thickness depends on the duration of plasma treatment [20],[43].

In our case, we have investigated PDMS1 surface chemistry immediately after plasma oxygen in ICP for 15s considering the time of exposure used during the fabrication of the scaffolds. At first glance, Raman spectra shown in Figure 4.c demonstrate an extensive change in the peak intensity so much as they disappear in some

Raman shift. In the range of 200-800cm$^{-1}$ (Figure 4.c.1), the peaks disappear after the treatment. For example, we cannot see the Si-O-Si peak, probably as a consequence of the breaking of the Si-O bond and the formation of Si-$O_x$ on the surface [44].

The peaks related to Si-$CH_3$ symmetric rocking, Si-C symmetric stretching and Si-$CH_3$ asymmetric rocking, also sharply decrease till they bled. This could be due to the modification of the surface by the exposure of the oxygen plasma. In the range of 1200-1600cm$^{-1}$ (Figure 4.c.2) the peak at 1261cm$^{-1}$ of $CH_3$ symmetric bending disappears whereas the peak at 1406cm$^{-1}$ for $CH_3$ asymmetric bending is shifted by almost 20cm$^{-1}$. This suggests a structural rearrangement of PDMS has occurred after plasma oxygen.

### *3.3 Surface wettability*

PDMS is inherently hydrophobic because of its chemical composition (repeating monomeric unit -OSi($CH_3$)-) and presents a contact angle in the order of 120° [45]. Several strategies have been employed so far to modify PDMS surface for biomedical systems and improve cell-surface adhesion. They can be divided into mechanical treatments such as plasma treatment [46], UV-ozone [45] and corona discharge [47] or chemical functionalization such as silanization [23],[48],[49] or chemical stabilization [49]. However, PDMS shows a fast "hydrophobic recovery" (in hours) after hydrophilization, and this is mainly attributed to its low glass transition temperature of less than -120°C, whereby low molecular weight hydrophobic oligomers are free to migrate from the bulk to the surface increasing the contact angle [50]. Hydrophobic recovery is also affected by a variety of experimental conditions such as sample thickness, curing conditions, vacuum treatment conditions and plasma treatment time [40].

In this work, we have used oxygen plasma treatment of PDMS1 since it is a fast method, compatible with microfabrication techniques and it increases the biocompatibility [50]. Also, since the hydrophobic recovery of PDMS is elusive, the wettability of PDMS1 has been monitored measuring the contact angle after preparation, immediately after plasma oxygen and for seven days. RIE and ICP were used and compared using the same exposure time but different plasma power.

Pristine PDMS1 shows its hydrophobicity with contact angle 122.9 ± 2.36° (Figure 5.a). After oxygen plasma (day 0) the contact angle decreases to 26.3 ± 4.1° for ICP and 25.73 ± 5.35° for RIE. These values are almost comparable at day 0. On the contrary, at the day one after the treatment PDMS1 treated with ICP showed a more hydrophilic surface with a contact angle of 31.07 ± 5.35° in comparison to the RIE with 54.70 ± 6.30° as contact angle (Figure 5.b,c). In Figure 5.d it is shown the trend of the contact angle of PDMS1 for seven days, and apart the day 0 ICP results in more effective treatment with a lower contact angle in comparison to RIE treatment. This means that the high-power plasma process causes long-term hydrophilicity consistently with the literature [42].

The roughness of the plasma oxidised PDMS1 immediately after RIE, and ICP treatments have also been evaluated using AFM. Results revealed that the exposure to oxygen plasma decreases the roughness consistently with the literature [40] and values are reported in Supplementary Figure S2.

The contact angle of PDMS1 employed on PP2 scaffolds after three days from a strong plasma treatment (ICP) remains almost constant with a value below 60° that was demonstrated to be good for cell adhesion [51],[52]. This result is advantageous for promoting cell adhesion.

When a liquid droplet is placed on a wavy surface with sinusoidal ripples, it wets anisotropically with a smaller contact angle perpendicular ($\theta_\perp$) to the direction of the grooves and larger contact angle parallel to the grooves ($\theta_{//}$) [53],[54],[55]. In this work, we have also examined the wettability of PP1 scaffolds. In Figure 6. a,b is shown the schematic convention used to measure $\theta_\perp$ (position of PP1 orthogonal to the camera) and $\theta_{//}$

(position of PP1 parallel to the camera). PP1 samples were treated using RIE for 15s, and the contact angle has been monitored for 6 days.

Before the treatment, the values of the contact angles of PP1 are comparable with 112.8 ± 6.8° and 104.43 ± 9.3° for $\theta_{//}$ and $\theta_{\perp}$ respectively (Figure 6.c,d). Immediately after the oxygen plasma (day 0) $\theta_{//}$ and $\theta_{\perp}$ sharply drop (Figure 6.e,f) and $\theta_{//}$ is larger (26.2 ± 2.8°) than $\theta_{\perp}$ (11.5 ± 1.2°). As shown in Figure 6.g we find that $\theta_{//}$ is larger than $\theta_{\perp}$ up to 4 days and they start to be similar at the day 5 after the treatment, but still lower than the untreated substrate. After 6 days PDMS1 samples recover the hydrophobicity with $\theta_{//}$ equal to 79.90 ± 10.31° and $\theta_{\perp}$ equal to 78.53 ± 6.06°.

The PP1 scaffolds, after three days from a mild treatment (RIE), show a contact angle almost constant with a value of 80°, still good for cell adhesion. The substrates with a contact angle of 80° are considered weakly hydrophobic [56] and this value of contact angle can be still considered good for promoting cell adhesion as reported by Trantidou et al. in [51].

### *3.4 Young's modulus evaluation*

The elasticity of scaffolds has a profound effect on cell spreading, morphology and function [23].

The mechanical characterisation of polymers at the nanoscale sometimes leads to models (e.g. Oliver and Pharr) that cannot estimate the real values of Young's modulus unless the analysis is limited to a penetration depth where the contact between the tip and the material is perfectly elastic. The reason for this failure can be found in the inhomogeneity of the polymeric structure of the polymers; pile-up and sink-in phenomena [57] may also occur changing the nanoindentation contact. Even though different mathematical models were applied to correctly determine Young's modulus from a variety of nanoindentation methods (for example introducing a correction factor), AFM results in the most appropriate nanoindentation technique to adopt [58].

In this work, we have employed AFM force-distance curves to study the mechanical properties of PDMS bulk and PDMS thin films. We have assumed that the elastic modulus can be affected by the spin coating process. Therefore, we have tested the mechanical properties of the material with different thickness because in this work we have spin-coated PDMS for the microfabrication of the scaffolds. In Figure 7 a,b,c,d, some representative force-distance curves of different films are shown.

Force-distance curves show strong adhesion forces ( from 27 to 56nN), especially in the unloading part (pull-off force), that appear to be influenced by the probe state. We have observed the same experimental evidence made by E. Kroner et al. [59], where during the first contact the adhesion force is lower than the second contact maybe because some free oligomers are pulled out from the sample and transferred on the tip [59].

Based on the force-distance curves obtained, the DMT model is the most appropriate model to evaluate Young's modulus [60]. Table S3 in Supporting Information presents all the mean values extracted from force-distance curves. Our results demonstrate that spin-coating does not affect the elastic properties of the material and the values of Young's moduli we have found are close to the expected value (almost 1MPa) for all the samples.

### *3.5 Hybrid scaffolds effects on NRVM alignment*

After fabrication and materials characterisation, the application of scaffolds was investigated considering the effect on morphological changes and alignment of NRVMs. Cells were cultured on HH, PP1 and PP2 scaffolds. HH scaffolds were used as a control since they have been reported in previous studies as good scaffolds for NRVMs alignment [2]. However, the elasticity of HH scaffolds is not close to the elastic modulus of the natural extracellular environment. This is the reason why PDMS was applied as scaffolding

material to fabricate PP1 and PP2 scaffolds which have in common the height and the elasticity closer to the heart tissue [51],[30]. In addition, PP2 scaffolds have the advantage to have a hybrid surface with stiff and soft areas.

At first glance, fluorescence images showed that cells were well-aligned only on HH and PP2 scaffolds (Figure 8.a,b,c). PP2 scaffolds yielded cell alignment in the direction of the grooves with cells forming a monolayer in compared to PP1 scaffolds where cells were more randomly distributed forming structures like clusters (Figure 8.d). Cells on HH scaffolds showed a more tubular morphology with sarcomere striation whereas cells seeded on PP2 presented less striation with elongated myofibrils. We believe that the alignment of mature myofibrils on PP2 scaffolds is due to the combination of the surface chemistry and mechanical properties of the soft regions. On the contrary, on the HH scaffolds cells are anisotropically guided only by the hydrophilic regions. In fact, it has been demonstrated that cardiomyocytes present an organized myofibrillar architecture on soft substrates with a stiffness close to the native tissue[18], [61]. Since the topography of HH and PP2 scaffolds was almost the same, results suggested that the cells behaved in a similar manner on such similar topographies. Moreover, the alignment of NRVMs on these scaffolds did not reveal a significant difference, as showing in Figure 8.d (average values of nuclei alignment of NRVMs on HH is 27.82 ± 6.36° and 37.74 ± 8.23° for PP2).

Cells seeded on the PP1 scaffolds (Figure 8.e) showed a random orientation with an angle of 39.98 ± 10.7°. This evidence can be attributed to the structures of the surface. Results reported in the literature demonstrate that myocytes can sense the microscale topography developing an alignment in the preferential direction even if it is a wavy surface [5]. According to the work of Lam et al., myotubes on wavy PDMS with ripples of 1.7 μm height and wavelength 12 μm can show high orientation angles rather than cells growth on shallow waves (300 nm deep) and lower wavelength (~3 μm) [12].

The general way to report cardiomyocyte morphology is the aspect ratio. This value for cardiomyocytes typically ranges from 1.3 to 5 in vitro depending on the stiffness of the substrates [15]. The aspect ratio reported in Figure 3.22.e evaluated on 25 cells confirmed that NRVMs on PP1 scaffolds have a lower elongation with a lower aspect ratio. Cells on HH and PP2 showed greater elongation and wise spreading in comparison to cells on PP1.

Cell area was also investigated, and results reported an average value of 323.22 ± 161.90 $\mu m^2$ for HH scaffolds and 242.05 ± 108.67 $\mu m^2$ for PP1. Cells on PP2 revealed an area of 354.83 ± 213.17 $\mu m^2$ higher in comparison to cells seeded on HH and PP1. Cell area distribution was more negatively skewed across the average value for HH and PP1 scaffolds than PP2 ones.

From these preliminary observations, PP2 scaffolds reveal a preferential cell orientation with a morphology comparable to the cells seeded on the control (HH scaffolds). Based on these results, PP2 scaffolds can be further considered to study the effect of the elasticity on cell activity. In fact, PP2 have many advantages compared to HH for further applications in cardiac *in vitro* models. Firstly, from the fabrication point of view, the technique proposed is versatile and can be employed to fabricate scaffolds with a controllable topography and elasticity, for example by changing the height of the grooves or by changing the polymeric composition of PDMS. Secondly, the PP2 scaffolds have the unique properties to present a hybrid architecture made from elastic/hydrophilic and hydrophobic/stiff regions that were observed to be successful to align cells. Thirdly, PP2 scaffolds would provide a more realistic and versatile platform for in vitro models because they are more elastic than HH scaffolds. Finally, PP2 scaffolds have the advantage to be peeled-off from the substrates and be applied in the future to investigate the functional activity of cells such as self-beating.

PP1 showed a random distribution with not mature morphology of cells. However, the applicability of PP1 cannot be excluded in cardiac tissue engineering because we believe that they represent a realistic platform

with elasticity and topography close to the heart tissue. PP1 need more investigation since this type of topographies have been less investigated on NRVMs alignment.

## 4 Conclusions

One of the most challenging goals in cardiac TE is to recreate anisotropic milieus at the micro- and nano-scale by using techniques suitable to shape biocompatible polymers. In this work, we provide a new strategy to pattern 2D anisotropic features on PDMS. Parylene C films, more rigid, were mainly used as a template to form an anisotropic grating on PDMS that was considered particularly suitable for the cell-polymer interface.

We have demonstrated that hybrid scaffolds can be easily prototyped without sophisticated techniques and with high repeatability. PDMS can be spin coated to form thin membranes down to 8µm without changing its chemical and mechanical properties. The effect of oxygen plasma on PDMS was also investigated, and we have monitored the wettability demonstrating that ICP at the power of 1000W renders a more effective hydrophilisation than RIE at 200W. The wettability of our PDMS samples with microscale wrinkle structures was also studied, indicating similar retention (~ 6 days) for both contact angles (parallel and perpendicular).

Finally, the scaffolds were seeded with NRVMs to study the effect of the topography on the alignment. Among all the scaffolds, PP2 ones demonstrated a better alignment of cells compared with the control (HH scaffolds) with cells exhibiting a better myofibril reassembly.

Scaffolds with a corrugated topography have induced a random distribution of cells with high orientation angle in comparison to the other two scaffolds where cells have aligned with a mature morphology.

In conclusion, PP1 scaffolds with corrugated topographies need more investigation to be applied for NRVM for *in vitro* models, while micro-grooved hybrid scaffolds may be useful in engineering cardiac tissue to study the effect of the elasticity on the contractile activity of cells.

**Acknowledgements**

The authors wish to thank Dr Norman Godinho for his financial support.

**References**

[1] C. Rao *et al.*, “The effect of microgrooved culture substrates on calcium cycling of cardiac myocytes derived from human induced pluripotent stem cells,” *Biomaterials*, vol. 34, no. 10, pp. 2399–2411, 2013.

[2] T. Trantidou, C. M. Terracciano, D. Kontziampasis, E. J. Humphrey, and T. Prodromakis, “Biorealistic cardiac cell culture platforms with integrated monitoring of extracellular action potentials,” *Sci. Rep.*, vol. 5, no. November 2014, p. 11067, 2015.

[3] J. Ballester-BeltrÃ¡n, M. J. P. Biggs, M. J. Dalby, M. SalmerÃ$^{3}$n-SÃ¡nchez, and A. Leal-EgaÃ±a, “Sensing the Difference: The Influence of Anisotropic Cues on Cell Behavior,” *Front. Mater.*, vol. 2, no. May, pp. 1–12, 2015.

[4] L. Yin, H. Bien, and E. Entcheva, “Scaffold topography alters intracellular calcium dynamics in cultured cardiomyocyte networks.,” *Am. J. Physiol. Heart Circ. Physiol.*, vol. 287, no. 3, pp. H1276–H1285, 2004.

[5] L. Altomare, N. Gadegaard, L. Visai, M. C. Tanzi, and S. Farè, “Biodegradable microgrooved polymeric surfaces obtained by photolithography for skeletal muscle cell orientation and myotube development,” *Acta Biomater.*, vol. 6, no. 6, pp. 1948–1957, 2010.

[6] T. Trantidou *et al.*, “Selective hydrophilic modification of Parylene C films: a new approach to cell micro-patterning for synthetic biology applications.,” *Biofabrication*, vol. 6, no. 2, p. 25004, 2014.

[7] F. Di Benedetto, A. Biasco, D. Pisignano, and R. Cingolani, "Patterning polyacrylamide hydrogels by soft lithography," *Nanotechnology*, vol. 16, no. 5, pp. S165–S170, 2005.
[8] M. Kitsara, O. Agbulut, D. Kontziampasis, Y. Chen, and P. Menasché, "Fibers for hearts: A critical review on electrospinning for cardiac tissue engineering," *Acta Biomater.*, vol. 48, pp. 20–40, 2017.
[9] H. Bien, L. Yin, and E. Entcheva, "Cardiac Cell Networks on Elastic Microgrooved Scaffolds," *IEEE Eng. Med. Biol. Mag.*, vol. 22, no. 5, pp. 108–112, 2003.
[10] D.-H. Kim *et al.*, "Nanoscale cues regulate the structure and function of macroscopic cardiac tissue constructs.," *Proc. Natl. Acad. Sci. U. S. A.*, vol. 107, no. 2, pp. 565–570, 2010.
[11] M. Nikkhah, F. Edalat, S. Manoucheri, and A. Khademhosseini, "Engineering microscale topographies to control the cell-substrate interface," *Biomaterials*, vol. 33, no. 21, pp. 5230–5246, 2012.
[12] N. F. Huang *et al.*, "Myotube assembly on nanofibrous and micropatterned polymers," *Nano Lett.*, vol. 6, no. 3, pp. 537–542, 2006.
[13] F. Asghari, M. Samiei, K. Adibkia, A. Akbarzadeh, and S. Davaran, "Biodegradable and biocompatible polymers for tissue engineering application: a review.," *Artif. cells, nanomedicine, Biotechnol.*, vol. 1401, pp. 1–8, 2016.
[14] M. T. Lam, S. Sim, X. Zhu, and S. Takayama, "The effect of continuous wavy micropatterns on silicone substrates on the alignment of skeletal muscle myoblasts and myotubes," *Biomaterials*, vol. 27, no. 24, pp. 4340–4347, 2006.
[15] I. Sanzari, M. Callisti, A. De Grazia, D. J. Evans, T. Polcar, and T. Prodromakis, "Parylene C topographic micropattern as a template for patterning PDMS and Polyacrylamide hydrogel," *Sci. Rep.*, vol. 7, no. 1, p. 5764, 2017.
[16] A. J. Engler, M. a. Griffin, S. Sen, C. G. Bönnemann, H. L. Sweeney, and D. E. Discher, "Myotubes differentiate optimally on substrates with tissue-like stiffness: Pathological implications for soft or stiff microenvironments," *J. Cell Biol.*, vol. 166, no. 6, pp. 877–887, 2004.
[17] J. G. Jacot, A. D. McCulloch, and J. H. Omens, "Substrate stiffness affects the functional maturation of neonatal rat ventricular myocytes.," *Biophys. J.*, vol. 95, no. 7, pp. 3479–3487, 2008.
[18] M. Tallawi, R. Rai, A. R. Boccaccini, and K. Aifantis, "Effect of substrate mechanics on cardiomyocyte maturation and growth.," *Tissue Eng. Part B. Rev.*, vol. 21, no. 1, pp. 157–165, 2014.
[19] R. Seghir and S. Arscott, "Controlled mud-crack patterning and self-organized cracking of polydimethylsiloxane elastomer surfaces," *Sci. Rep.*, vol. 5, no. October, pp. 1–16, 2015.
[20] K. Tsougeni, A. Tserepi, G. Boulousis, V. Constantoudis, and E. Gogolides, "Control of nanotexture and wetting properties of polydimethylsiloxane from very hydrophobic to super-hydrophobic by plasma processing," *Plasma Process. Polym.*, vol. 4, no. 4, pp. 398–405, 2007.
[21] J. Tong, C. a Simmons, and Y. Sun, "Precision patterning of PDMS membranes and applications," *J. Micromechanics Microengineering*, vol. 18, no. 3, p. 037004, 2008.
[22] C. De Menezes Atayde and I. Doi, "Highly stable hydrophilic surfaces of PDMS thin layer obtained by UV radiation and oxygen plasma treatments," *Phys. Status Solidi Curr. Top. Solid State Phys.*, vol. 7, no. 2, pp. 189–192, 2010.
[23] K. M. Broughton and B. Russell, "Cardiomyocyte subdomain contractility arising from microenvironmental stiffness and topography," *Biomech. Model. Mechanobiol.*, pp. 589–602, 2014.
[24] J. E. Sader, I. Larson, P. Mulvaney, and L. R. White, "Method for the calibration of atomic force microscope cantilevers," *Rev. Sci. Instrum.*, vol. 66, no. 7, pp. 3789–3798, 1995.
[25] R. Suriano, C. Credi, M. Levi, and S. Turri, "AFM nanoscale indentation in air of polymeric and hybrid materials with highly different stiffness," *Appl. Surf. Sci.*, vol. 311, pp. 558–566, 2014.
[26] D. C. Lin, E. K. Dimitriadis, and F. Horkay, "Elasticity of rubber-like materials measured by AFM nanoindentation," *Express Polym. Lett.*, vol. 1, no. 9, pp. 576–584, 2007.
[27] Z. Wang, A. a. Volinsky, and N. D. Gallant, "Nanoindentation study of polydimethylsiloxane elastic modulus using berkovich and flat punch tips," *J. Appl. Polym. Sci.*, vol. 132, no. 5, pp. 1–7, 2015.
[28] B. Cappella and G. Dietler, "Force-distance curves by atomic force microscopy," *Surf. Sci. Rep.*, vol. 34, no. 1–3, pp. 1–104, 1999.
[29] C. Rao *et al.*, "The effect of microgrooved culture substrates on calcium cycling of cardiac myocytes derived from human induced pluripotent stem cells," *Biomaterials*, vol. 34, no. 10, pp. 2399–2411, 2013.
[30] C. Rao, "The effect of biomimetic tissue engineering constructs on the phenotype of immature

cardiomyocytes," no. September, 2013.
[31] C. Rao *et al.*, "The effect of microgrooved culture substrates on calcium cycling of cardiac myocytes derived from human induced pluripotent stem cells," *Biomaterials*, vol. 34, no. 10, pp. 2399–2411, 2013.
[32] G. J. Scuderi and J. Butcher, "Naturally Engineered Maturation of Cardiomyocytes," vol. 5, no. May, pp. 1–28, 2017.
[33] C. J. Bettinger, R. Langer, and J. T. Borenstein, "Minireviews Engineering Substrate Topography at the Micro- and Nanoscale to Control Cell Function," pp. 5406–5415, 2009.
[34] N. Heart, "Effect of patterned polyacrylamide hydrogel on morphology and orientation of cultured NRVMs," pp. 1–12, 2018.
[35] M. Liu, J. Sun, Y. Sun, C. Bock, and Q. Chen, "Thickness-dependent mechanical properties of polydimethylsiloxane membranes," *J. Micromechanics Microengineering*, vol. 19, no. 3, p. 035028, 2009.
[36] D. A. Strubbe, E. C. Johlin, T. R. Kirkpatrick, T. Buonassisi, and J. C. Grossman, "Stress effects on the Raman spectrum of an amorphous material: Theory and experiment on a -Si:H," *Phys. Rev. B - Condens. Matter Mater. Phys.*, vol. 92, no. 24, pp. 1–6, 2015.
[37] A. M. Alshehri, K. L. N. Deepak, D. T. Marquez, S. Desgreniers, and V. R. Bhardwaj, "Localized nanoclusters formation in PDMS upon irradiation with femtosecond laser," *Opt. Mater. Express*, vol. 5, no. 4, pp. 858–869, 2015.
[38] M. R. Gonçalves, F. Enderle, and O. Marti, "Surface-enhanced Raman spectroscopy of dye and thiol molecules adsorbed on triangular silver nanostructures: A study of near-field enhancement, localization of hot-spots, and passivation of adsorbed carbonaceous species," *J. Nanotechnol.*, vol. 2012, 2012.
[39] D. A. Long, "Infrared and Raman characteristic group frequencies. Tables and chartsGeorge Socrates John Wiley and Sons, Ltd, Chichester, Third Edition, 2001. Price £135," *J. Raman Spectrosc.*, vol. 35, no. 10, pp. 905–905, 2004.
[40] S. H. Tan, N. T. Nguyen, Y. C. Chua, and T. G. Kang, "Oxygen plasma treatment for reducing hydrophobicity of a sealed polydimethylsiloxane microchannel," *Biomicrofluidics*, vol. 4, no. 3, pp. 1–8, 2010.
[41] M. M. Stanton, J. M. Rankenberg, B.-W. Park, W. G. McGimpsey, C. Malcuit, and C. R. Lambert, "Cell behavior on surface modified polydimethylsiloxane (PDMS).," *Macromol. Biosci.*, vol. 14, no. 7, pp. 953–64, 2014.
[42] D. Bodas and C. Khan-Malek, "Formation of more stable hydrophilic surfaces of PDMS by plasma and chemical treatments," *Microelectron. Eng.*, vol. 83, no. 4–9 SPEC. ISS., pp. 1277–1279, 2006.
[43] M. J. Owen and J. L. Stasser, "Plasma treatment of polydimethylsiloxane," *Am. Chem. Soc. Polym. Prepr. Div. Polym. Chem.*, vol. 38, no. 1, pp. 1087–1088, 1997.
[44] H. G. Park, H. C. Jeong, Y. H. Jung, and D. S. Seo, "Control of the wrinkle structure on surface-reformed poly(dimethylsiloxane) via ion-beam bombardment," *Sci. Rep.*, vol. 5, no. January, pp. 1–8, 2015.
[45] W. Hellmich, J. Regtmeier, T. T. Duong, R. Ros, D. Anselmetti, and A. Ros, "Poly(oxyethylene) based surface coatings for poly(dimethylsiloxane) microchannels," *Langmuir*, vol. 21, no. 16, pp. 7551–7557, 2005.
[46] a. Tserepi *et al.*, "Plasma Nanotextured Polymeric Surfaces for Controlling Cell Attachment and Proliferation: A Short Review," *Plasma Chem. Plasma Process.*, 2015.
[47] H. Hillborg and U. W. Gedde, "Hydrophobicity recovery of polydimethylsiloxane after exposure to corona discharges," *Polymer (Guildf).*, vol. 39, no. 10, pp. 1991–1998, 1998.
[48] Y. J. Chuah, S. Kuddannaya, M. H. A. Lee, Y. Zhang, and Y. Kang, "The effects of poly(dimethylsiloxane) surface silanization on the mesenchymal stem cell fate," *Biomater. Sci.*, vol. 3, no. 2, pp. 383–390, 2015.
[49] G. G. Genchi *et al.*, "Bio/non-bio interfaces: A straightforward method for obtaining long term PDMS/muscle cell biohybrid constructs," *Colloids Surfaces B Biointerfaces*, vol. 105, pp. 144–151, 2013.
[50] J. Zhou, A. V. Ellis, and N. H. Voelcker, "Recent developments in PDMS surface modification for microfluidic devices," *Electrophoresis*, vol. 31, no. 1, pp. 2–16, 2010.
[51] T. Trantidou, E. J. Humphrey, C. Poulet, J. Gorelik, T. Prodromakis, and C. M. Terracciano, "Surface

Chemistry and Microtopography of Parylene C Films Control the Morphology and Microtubule Density of Cardiac Myocytes," *Tissue Eng. Part C Methods*, vol. 22, no. 5, pp. 464–472, 2016.

[52] D. P. Dowling, I. S. Miller, M. Ardhaoui, and W. M. Gallagher, "Effect of surface wettability and topography on the adhesion of osteosarcoma cells on plasma-modified polystyrene," *J. Biomater. Appl.*, vol. 26, no. 3, pp. 327–347, 2011.

[53] C. M. Chen and S. Yang, "Wrinkling instabilities in polymer films and their applications," *Polym. Int.*, vol. 61, no. 7, pp. 1041–1047, 2012.

[54] J. Y. Chung, J. P. Youngblood, and C. M. Stafford, "Anisotropic wetting on tunable micro-wrinkled surfaces," *Soft Matter*, vol. 3, no. 9, p. 1163, 2007.

[55] K. Khare, J. Zhou, and S. Yang, "Tunable open-channel microfluidics on soft poly(dimethylsiloxane) (PDMS) substrates with sinusoidal grooves," *Langmuir*, vol. 25, no. 21, pp. 12794–12799, 2009.

[56] N. Vasilakis, D. Moschou, D. Carta, H. Morgan, and T. Prodromakis, "Long-lasting FR-4 surface hydrophilisation towards commercial PCB passive microfluidics," *Appl. Surf. Sci.*, vol. 368, pp. 69–75, 2016.

[57] A. S. Bhattacharyya *et al.*, "Substrate effect and nanoindentation fracture toughness based on pile up and failure," pp. 1–40.

[58] D. Tranchida, S. Piccarolo, J. Loos, and A. Alexeev, "Mechanical characterization of polymers on a nanometer scale through nanoindentationn. A study on pile-up and viscoelasticity," *Macromolecules*, vol. 40, no. 4, pp. 1259–1267, 2007.

[59] E. Kroner, R. Maboudian, and E. Arzt, "Adhesion characteristics of pdms surfaces during repeated pull-off force measurements," *Adv. Eng. Mater.*, vol. 12, no. 5, pp. 398–404, 2010.

[60] F. L. Leite, C. C. Bueno, A. L. Da Róz, E. C. Ziemath, and O. N. Oliveira, *Theoretical models for surface forces and adhesion and their measurement using atomic force microscopy*, vol. 13, no. 10. 2012.

[61] A. J. S. Ribeiro *et al.*, "Contractility of single cardiomyocytes differentiated from pluripotent stem cells depends on physiological shape and substrate stiffness," *Proc. Natl. Acad. Sci.*, vol. 112, no. 41, 2015.

**Table 1.** Thickness of PDMS fims.

**Table 2. Profilometric data for the three microstructured constructs.**

**Figure 1. Fabrication of PDMS/Parylene C based scaffolds (PP2).** PDMS is spin-coated on a glass substrate (a), cured in an oven (b) and covered with Parylene C (c). Standard optical lithography process was utilised (d-e) to selectively etch Parylene C and hydrophilize PDMS (f) to create hydrophilic PDMS areas with raised hydrophobic Parylene C ridges (g). A representative SEM image of the pattern is shown in (h) with red scale bar of 10 µm. In (i), (j) and (k) HH, PP1 and PP2 scaffolds seeded with NRVMs are illustrated. The fabrication process of HH and PP1 scaffolds is reported in [15] while the fabrication of PP2 is herein described in detail.

**Figure 2. Schematic of the AFM set-up used to test the mechanichal properties of PDMS (a) and scheme of tip-sample interaction during the approach of the tip to the sample (b).** The indentation depth results from the difference between the vertical movement and the cantilever deflection.

**Figure 3. Topographic images of the three scaffolds (a-c) and the corresponding height profiles (d-f).**

**Figure 4. Raman spectra of PDMS plain surfaces at different spin coating and after oxygen plasma treatment.** Raman spectra of PDMS thin films obtained at different spin-coating (a). In b) is shown a sketch of surface chemistry modification of PDMS after oxygen plasma. In c) there are the Rama spectra of pristine and un-treated PDMS1. Raman spectra zoom is shown in d) with spectra windows: 200-800 $cm^{-1}$ (1) and 1200-1600$cm^{-1}$ (2) with Raman peak shift (around 1406$cm^{-1}$)).

**Figure 5. Comparison of hydrophilicity restoration of PDMS1 after RIE and ICP treatment.** The static contact angle of 5µl water drops on flat PDMS1 before oxygen plasma and 1 day after the treatment with RIE and ICP (a, b, c). A comparison between PDMS1 samples differently treated with oxygen plasma generated by RIE and ICP (d).

**Figure 6. Contact angle measurements on PP1 substrates in two different directions (parallel ($\theta_{//}$) and perpendicular ($\theta_{\perp}$) from the side view).** Schematic illustration of the contact angle measurements on the grooved structures in orthogonal (a) and parallel direction (b). The shape of water droplets on perpendicular and parallel direction before oxygen plasma (c,d) and immediately after the treatment (e,f). In g) contact angle measurements of PP1 samples in both perpendicular and parallel directions as a function of time are compared. (The error bar indicates the standard deviation of the mean value).

**Figure 7. Representative force-distance curves acquired during indentation tests for PDMS bulk (a) and PDMS thin films (b-d).**

**Figure 8. Cell alignment on engineered hybrid constructs.** In a) there are representative fluorescent micrographs of NRVMs aligned on HH constructs at two different magnifications (4x and 40x), in b) cells aligned on PP2 and in c) NRVMs randomly distributed on PP1. In d) an immunofluorescence image of cells cultured on PP1 that forms a blob. In e) the moduli of angle of nuclei from mean axis, aspect ratio and area is shown for the three scaffolds. Notes: white arrow: direction of the pattern; white scale bar: 50 μm; yellow scale bar: 50 μm; green labelling: Cx43 expression; * $p \pm 0.05$; ** $p \pm 0.01$.

Table 1

| **Sample** | **Thickness** [a] |
|---|---|
| PDMS bulk | ~ 1mm |
| PDMS0.5 | 32.96 ± 1.2 µm |
| PDMS1 | 22.06 ± 1.8 µm |
| PDMS4 | 13.66 ± 0.45 µm |
| PDMS6 | 8.49 ± 0.17 µm |

[a]Measured by a stylus profiler on a step created on the surface of the same sample.

Table 2

| **Scaffold** | **Ridge (µm)** | **Groove (µm)** | **Pitch/wavelength (µm)** | **Depth (µm)** |
|---|---|---|---|---|
| HH | 8.95±0.45 | 6.84±0.57 | 18.13 ± 0.6 | 0.89 ± 0.01 |
| PP1 | - | - | 20.23 ± 0.13 | 0.94 ± 0.11 |
| PP2 | 9.45 ± 0.59 | 5.36 ± 1.23 | 17.10 ± 0.67 | 0.63 ± 0.15 |

Figure 1

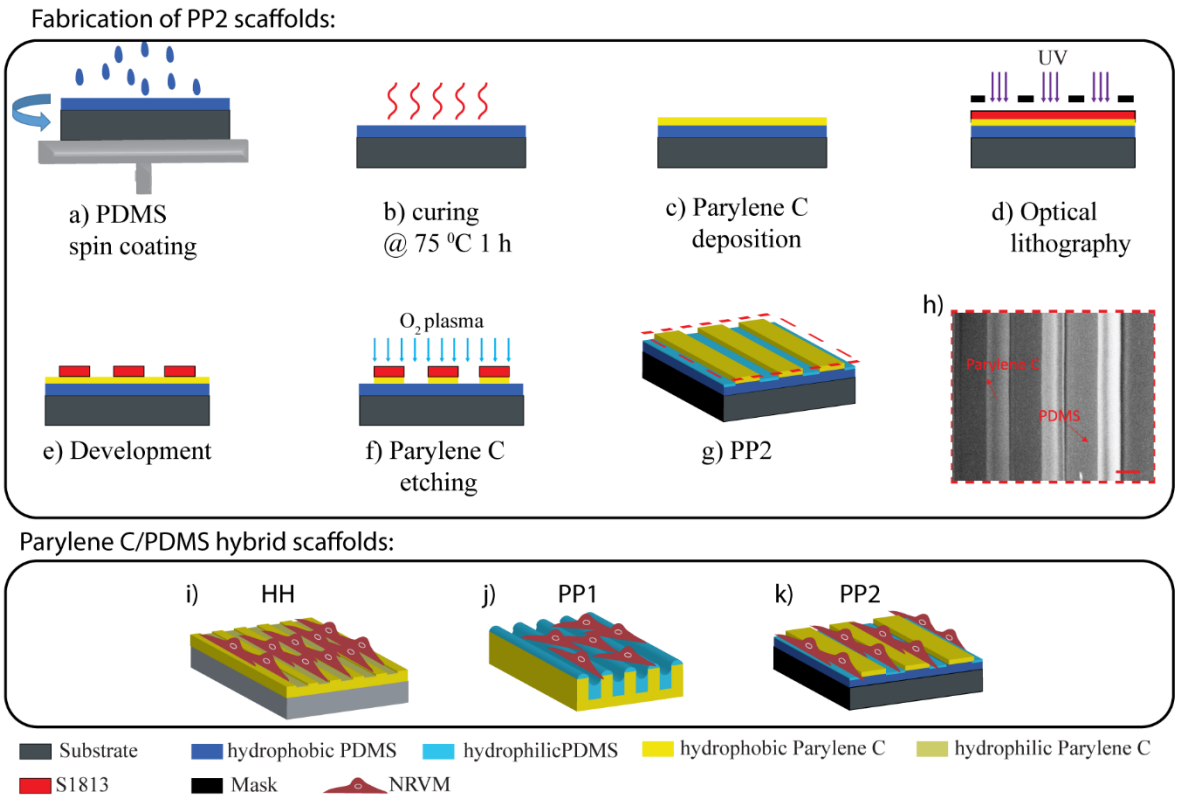

Figure 2

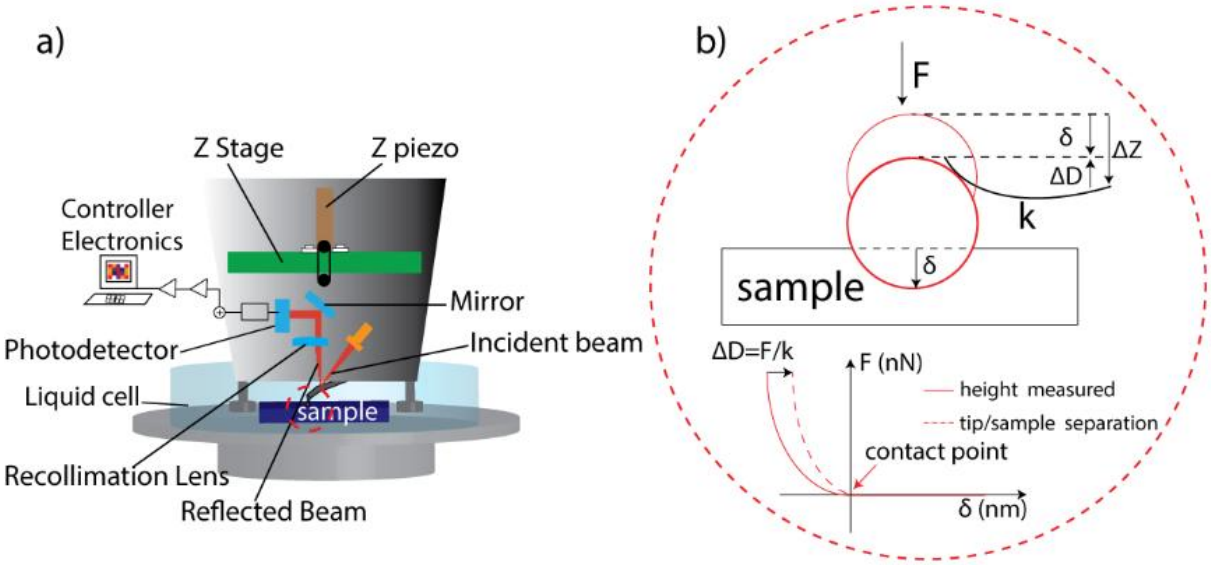

Figure 3

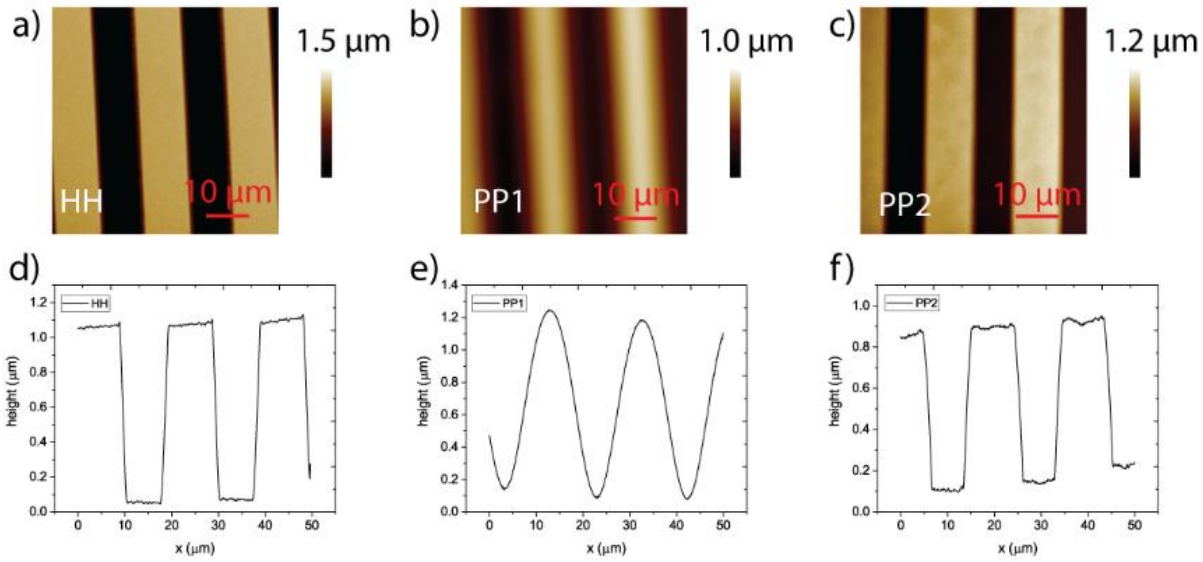

Figure 4

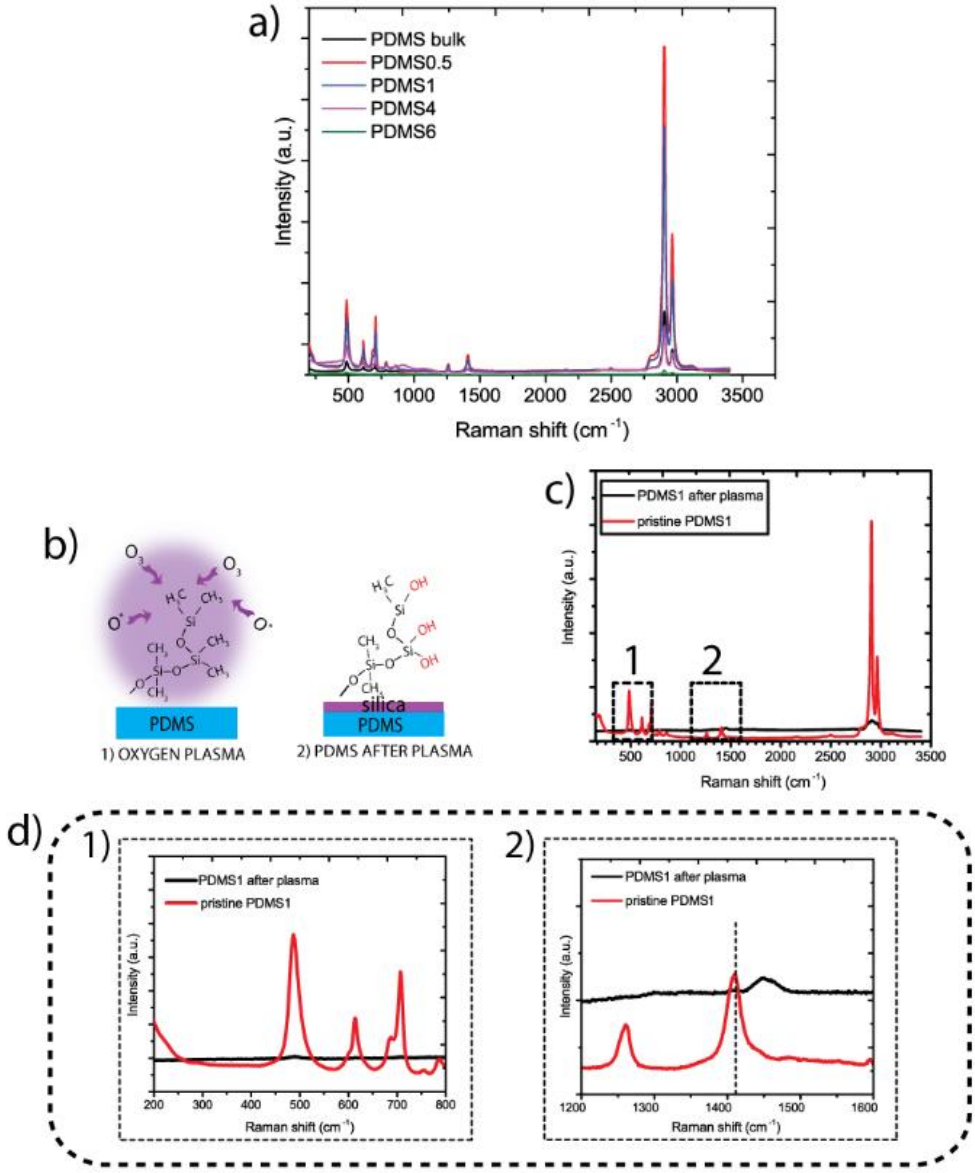

Figure 5

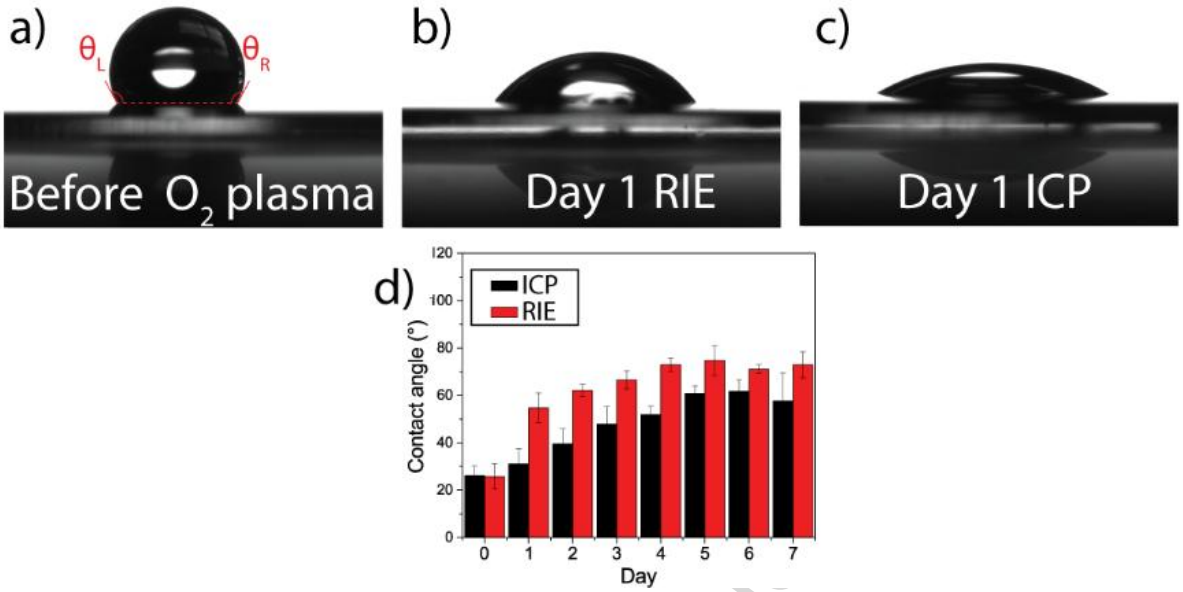

Figure 6

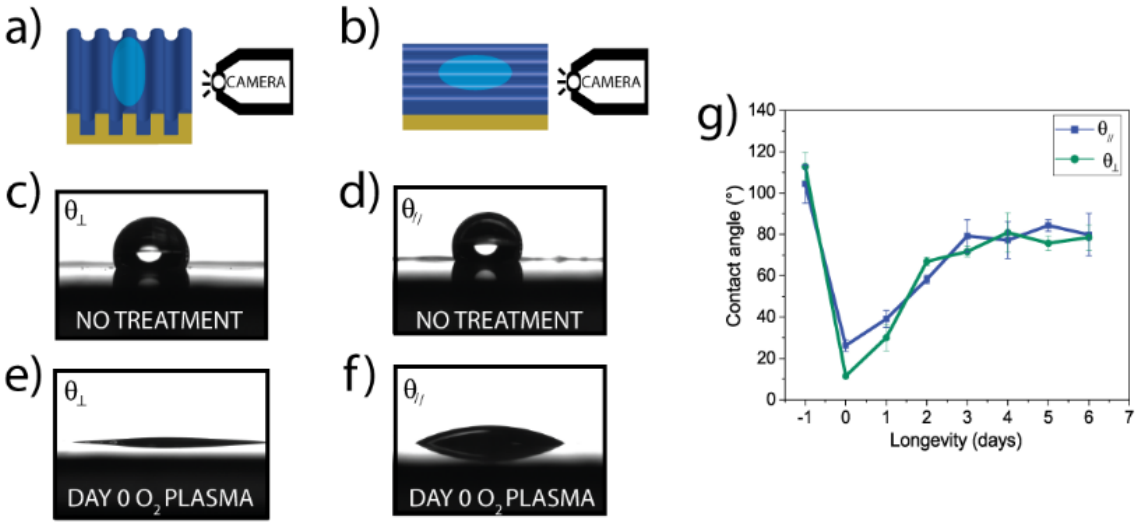

Figure 7

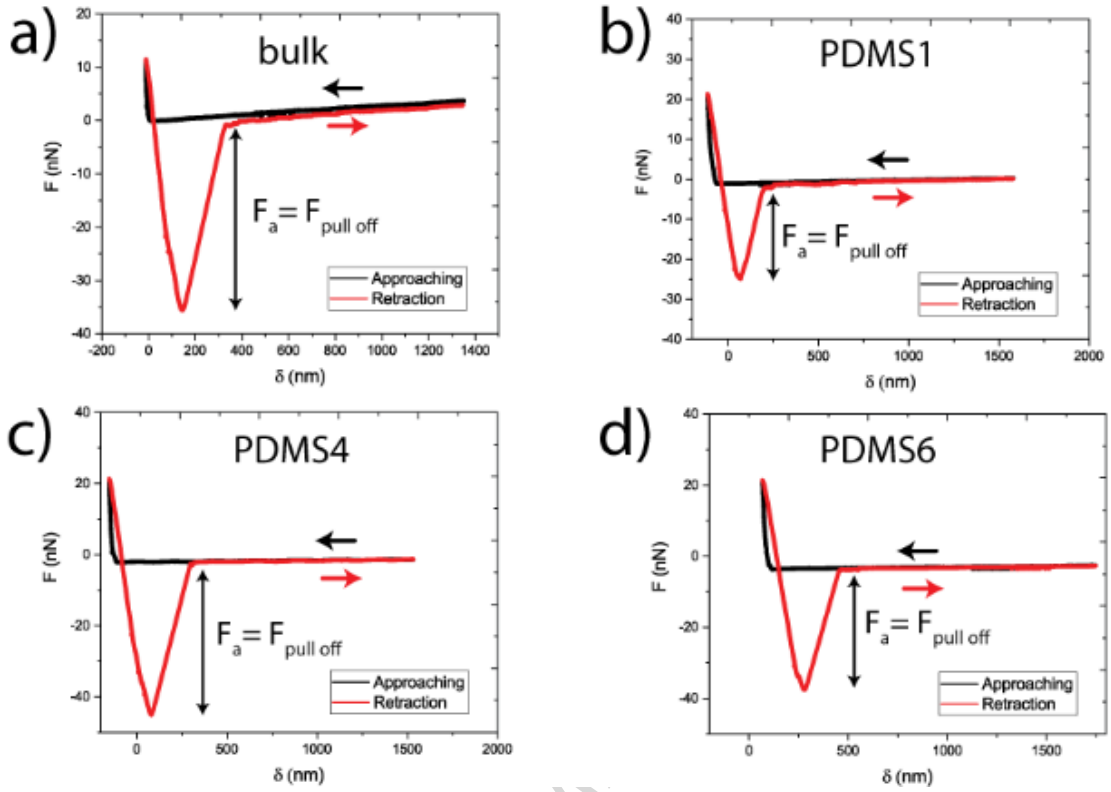

Figure 8

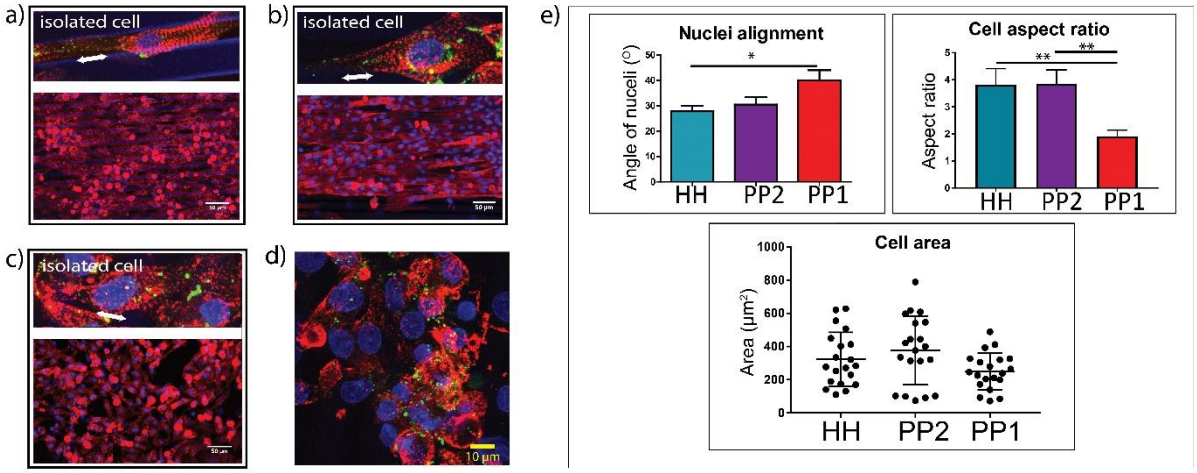

Graphical abstract

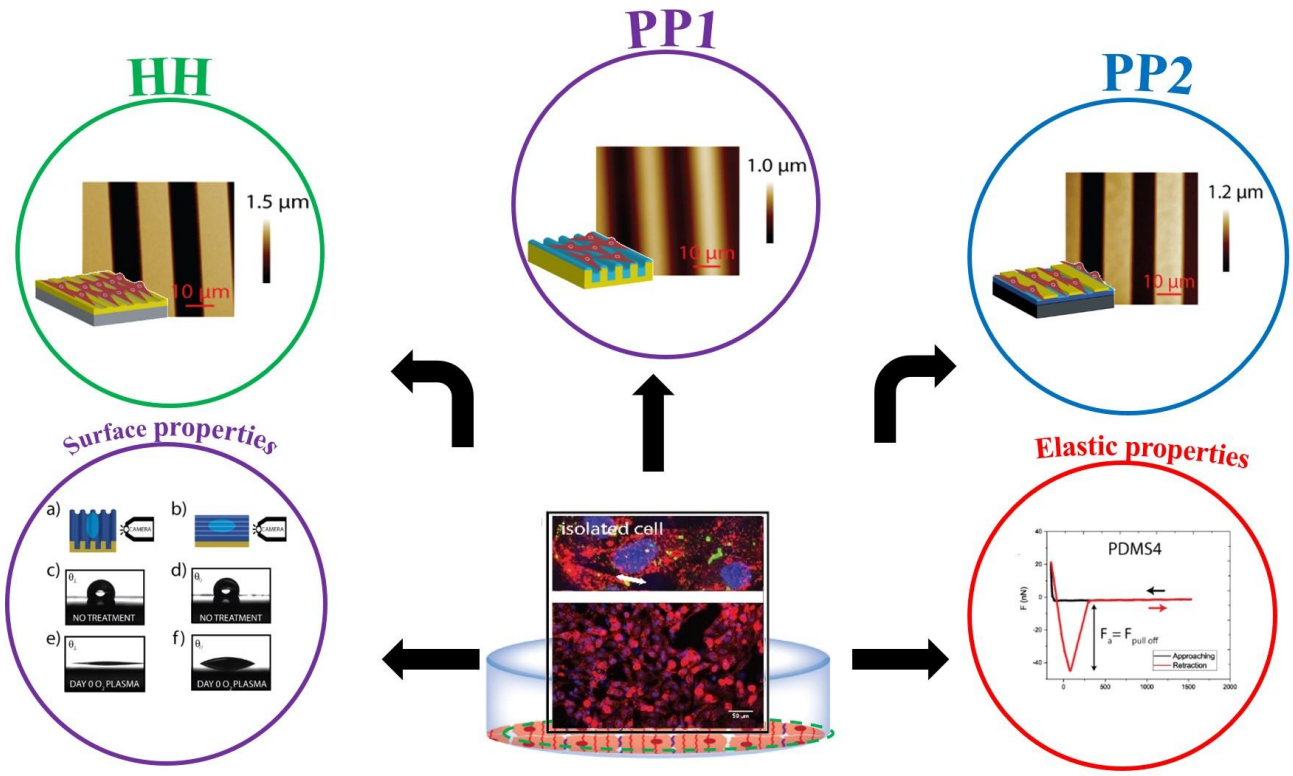

Highlights

1) Three hybrid anisotropic scaffolds based on Parylene C and PDMS were fabricated considering PDMS as material to be interfaced with cells
2) The chemical and physical properties of PDMS were investigated
3) The hypothesis that spin-coating was affected the mechanical properties of the PDMS thin films was verified
4) NRVMs alignment was studied on the three scaffolds